Eur. Phys. J. C 48, 477–488 (2006)
DOI 10.1140/epjc/s10052-006-0027-3

THE EUROPEAN PHYSICAL JOURNAL C

Regular Article – Theoretical Physics

On radiative QCD backgrounds to exclusive $H \to b\bar{b}$ production at the LHC and a photon collider

V.A. Khoze[1,2,a], M.G. Ryskin[1,2], W.J. Stirling[1,3]

[1] Department of Physics and Institute for Particle Physics Phenomenology, University of Durham, Durham DH1 3LE, UK
[2] Petersburg Nuclear Physics Institute, Gatchina, St. Petersburg, 188300, Russia
[3] Department of Mathematical Sciences, University of Durham, Durham DH1 3LE, UK

Received: 13 July 2006 /
Published online: 17 November 2006 –

Abstract. Central exclusive Higgs boson production, $pp \to p \oplus H \oplus p$, at the LHC and s-channel resonant Higgs production in the photon-collider option of the ILC can provide a very important contribution to the comprehensive study of the Higgs sector. Especially attractive is the $b\bar{b}$ Higgs decay mode, which for certain MSSM scenarios may become *the* discovery channel in exclusive Higgs production at the LHC and the photon collider (PC). Strongly suppressed and controllable backgrounds is an obvious requirement for the success of these exclusive measurements. One of the main sources of background comes from additional gluon radiation which leads to a three-jet $b\bar{b}g$ final state. We perform an explicit calculation of the subprocesses $gg \to q\bar{q}g$ and $\gamma\gamma \to q\bar{q}g$, where the incoming particles are required to be in a $J_z = 0$ state and the two gluons form a colour singlet, and investigate the salient properties of these potentially important background processes.

1 Introduction

The identification of the Higgs boson(s) is one of the main goals of the LHC. Once the Higgs boson is discovered, it will be of primary importance to determine its spin and parity, and to measure precisely the mass, width and couplings. A comprehensive study of the whole Higgs sector, including precision mass and coupling measurements, spin and CP properties, will be the next stage. The conventional strategy to achieve this ambitious programme requires an intensive interplay between the LHC and the ILC (high-energy linear e^+e^- collider) [1] . The ILC would enable a comprehensive phenomenological profile of the Higgs sector to be obtained, see for example [2]. In particular, a unique possibility to produce neutral Higgs bosons exclusively as s-channel resonances is offered by the $\gamma\gamma$ Compton Collider option of the ILC, see for example [3–11] and references therein. Whilst awaiting the arrival of the ILC, there has been growing interest in recent years in the possibility to complement the standard LHC physics menu by adding forward proton taggers to the CMS and ATLAS experiments (see for example [12–22] and references therein).

While experimentally challenging, this would provide an exceptionally clean environment to search for, and to identify the nature of, the new objects at the LHC. One of the key theoretical motivations behind these recent proposals is the study of so-called 'central exclusive' Higgs boson production, $pp \to p \oplus H \oplus p$. The $\oplus$ signs are used to denote the presence of large rapidity gaps; here we will simply describe such processes as 'central exclusive', with 'double-diffractive' production being implied. In these exclusive processes there is no hadronic activity between the outgoing protons and the decay products of the central (Higgs) system. The predictions for exclusive production are obtained by calculating the diagram of Fig. 1 using perturbative QCD [13, 23, 24]. In addition, we have to calculate and include the probability that the rapidity gaps are not populated by secondary hadrons from the underlying event [25, 26].

There are three major reasons why central exclusive production is so attractive for Higgs studies. First, if the outgoing protons remain intact and scatter through small angles then, to a very good approximation, the primary active di-gluon system obeys a $J_z = 0$, CP-even selection rule [27–29]. Here J_z is the projection of the total angular momentum along the proton beam axis. This selection rule readily permits a clean determination of the quantum numbers of the observed Higgs resonance which will be dominantly produced in a scalar state. Secondly, because the process is exclusive, the energy loss of the outgoing protons is directly related to the mass of the central system, allowing a potentially excellent mass resolution, irrespective of the decay mode of the produced

[a] e-mail: valery@ip3-mail.dur.ac.uk

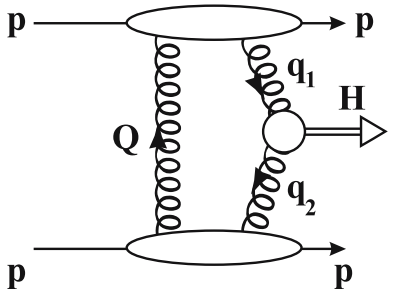

Fig. 1. Schematic diagram for central exclusive Higgs production at the LHC, $pp \to p + H + p$

particle[1]. And, thirdly, a signal-to-background ratio of order 1 (or even better) is achievable. As discussed in [31], central exclusive production would enable a unique signature for the MSSM Higgs sector, in particular allowing the direct measurement of the Hbb Yukawa coupling. Moreover, in some MSSM scenarios this mechanism provides an opportunity for lineshape analysing [16, 22], and offers a way for direct observation of a CP-violating signal in the Higgs sector [16, 32].

The analysis in [14, 22, 23] was focused primarily on light SM and MSSM Higgs production, with the Higgs decaying to 2 b-jets. The potentially copious b-jet (QCD) background is controlled by a combination of the $J_z = 0$ selection rule [27–29], which strongly suppresses leading-order $b\bar{b}$ production, colour and spin factors and the mass resolution from the forward proton detectors. It is the possibility to observe directly the dominant $b\bar{b}$ decay mode of the SM Higgs with $M_{\rm H} \lesssim 140\,{\rm GeV}$ that first attracted attention to exclusive production at the LHC. It was subsequently realised that certain regions of MSSM parameter space can be especially 'proton tagging friendly'. For example, at large $\tan\beta$ and $M_{\rm H} \lesssim 250\,{\rm GeV}$ the situation becomes exceptionally favourable, with predicted Higgs signal-to-background ratios in excess of 20 [22, 31]. In this particular case the tagged proton mode may well be *the* discovery channel. Though from an experimental perspective the $b\bar{b}$ channel is more challenging than the WW decay mode (see [33–35]), its unique advantages definitely merits a detailed analysis in realistic experimental conditions at the LHC.

At the same time, the PC is especially best suited to the precise measurement of the $\Gamma(H \to \gamma\gamma)$ width. Moreover, for certain regions of the MSSM parameter space, for example at the so-called 'LHC wedge', the PC has a discovery potential for the heavy pseudoscalar and scalar bosons, A and H, see for example [8–10]. It is instructive to recall that in the case of $\gamma\gamma \to H \to b\bar{b}$ production the potentially copious continuum b-jet background can be controlled by using polarised photon beams in the $J_z = 0$ initial-state (see for example [5, 36]), the same configuration of incoming particle polarisations that 'automatically' appears in the case of the pQCD box diagram of Fig. 1 for forward going protons at the LHC. The reason is that the Higgs signal is produced by photons (gluons) in a $J_z = 0$ state whereas the LO backgrounds are primarily initiated by the initial states with $|J_z| = 2$, the $J_z = 0$ contribution being suppressed for large angles by a factor m_b^2/s, see for example [36, 37]. As discussed in [38, 39] for the $\gamma\gamma$ case, the physical origin of this suppression is related to the symmetry properties of the Born helicity amplitudes $M^{\lambda_q,\lambda_{\bar{q}}}_{\lambda_1,\lambda_2}$ describing the binary background process

$$\gamma(\lambda_1, k_1) + \gamma(\lambda_2, k_2) \to q(\lambda_q, p) + \overline{q}(\lambda_{\bar{q}}, \overline{p})\,. \qquad (1)$$

Here λ_i labels the helicities of the incoming photons, and λ_q and $\lambda_{\bar{q}}$ are the (doubled) helicities of the produced quark and antiquark. The k's and p's denote the particle four-momenta, with $s = (k_1 + k_2)^2$.

Specifically, for a $J_z = 0$ initial state ($\lambda_1 = \lambda_2$) the Born quark helicity conserving (QHC) amplitude with $\lambda_{\bar{q}} = -\lambda_q$ vanishes,

$$M^{\lambda_q,-\lambda_q}_{\lambda,\lambda} = 0\,, \qquad (2)$$

see also [40]. For the quark helicity non-conserving (QHNC) amplitude for large angle production we have

$$M^{\lambda_q,\lambda_q}_{\lambda,\lambda} \sim \mathcal{O}\left(\frac{m_q}{\sqrt{s}}\right) M^{\lambda_q,-\lambda_q}_{\lambda,-\lambda}\,, \qquad (3)$$

where the amplitude on the right-hand-side displays the dominant helicity configuration of the background process. The above-mentioned m_b^2 suppression of the $\gamma\gamma(J_z = 0) \to b\bar{b}$ Born cross section is a consequence of (2) and (3). The same is valid for the leading order amplitude of the $gg^{\rm PP} \to b\bar{b}$ subprocess, where the notation $gg^{\rm PP}$ indicates that each active gluon in Fig. 1 comes from a colour-singlet t-channel (Pomeron) exchange and that the colour singlet di-gluon subprocess obeys the $J_z = 0$, parity-even selection rule[2].

The m_b^2/s suppression is especially critical in controlling the $b\bar{b}$ background. However, as was pointed out in [39], the suppression of the $J_z = 0$ background cross section is removed by the presence of an additional gluon in the final state. The radiative three-jet processes can then mimic the two-jet events in the quasi-collinear configurations when the gluon is radiated close to the b-quark directions[3] or (in the $gg^{\rm PP}$ case) the extra gluon goes unobserved in the direction of a forward proton. First evaluations of the NLO QCD radiative backgrounds at the PC were performed in [39, 40] (for further development see [8–10, 44] and references therein). This background

[1] Recent studies suggest [17] that the missing mass resolution σ will be of order 1% for a 140 GeV Higgs, assuming both protons are detected at 420 m from the interaction point [15, 30].

[2] It is worth noting that in the massless limit (2) holds for any colour state of initial gluons. This is a consequence of the general property that the non-zero massless tree-level amplitudes should contain at least two positive or two negative helicity states, see for example [41, 42]. It is an example of the more general maximally helicity violating amplitude (MHV) rule, reviewed for example in [43].

[3] In the PC case there also a sizeable radiative background coming from $c\bar{c}g$ production.

contribution appears to strongly exceed the LO expectation and results in different shapes for various distributions. The background situation for the central exclusive $H \to b\bar{b}$ production at the LHC is much more complicated and requires a detailed combined study of various effects, see [14, 18, 19]. The analysis of some of these phenomena is still incomplete and require further detailed theoretical efforts, see, in particular, Sects. 2.3 and 3 below.

An important ingredient to this complex study which has not been completed so far is the availability[4] of the analytical expression for the matrix elements of the NLO process $gg^{\rm PP} \to b\bar{b}g$ which are needed to perform explicit calculations of the radiative background in the presence of realistic experimental cuts and selections. It is one of the main aims of this paper to derive the analytical expressions for the radiative cross sections, which then can be convoluted with existing Monte Carlo codes [45, 46] for the calculation of central exclusive processes. Note that, technically, the calculations of both $gg^{\rm PP}$ and $\gamma\gamma$ induced colour singlet processes are quite similar, the latter providing just a subset of the diagrams for the former. Therefore, it is convenient to discuss the two radiative processes simultaneously, illuminating their similarities and differences. These are discussed in Sects. 3 and 4.

Our phenomenological discussion will be focused on central exclusive $b\bar{b}$ production at the LHC. However it is also worth noting that the CDF Collaboration at the Fermilab Tevatron is currently performing an experimental study of exclusive diffractive $b\bar{b}$ events [47, 48], and the results of this paper could prove useful for the analysis of these measurements.

2 On the backgrounds to the $p + (H \to b\bar{b}) + p$ signal

2.1 Classification of the backgrounds to exclusive Higgs production

From the theoretical point of view, it is convenient to consider separately the QHC and QHNC amplitudes. These amplitudes do not interfere, and their contributions can be treated independently. This could be especially convenient at the stage when the parton shower algorithm is applied, since double counting can be avoided.

There are two main sources of $gg^{\rm PP} \to b\bar{b}$ background process:

(i) the LO $\mathcal{O}(\alpha_{\rm S}^2)$ QHNC amplitude squared,
(ii) the NNLO $\mathcal{O}(\alpha_{\rm S}^4)$ QHC contribution which comes from the one-loop box diagrams.

As already mentioned, there is also the possibility of a NLO $\mathcal{O}(\alpha_{\rm S}^3)$ $gg^{\rm PP} \to b\bar{b}g$ background contribution, because large-angle, hard-gluon radiation does not obey the selection rules. Of course, the extra gluon may be observed experimentally in the central detector, and such background events eliminated. However, there are important exceptions which we discuss below.

In the case of the NLO $gg^{\rm PP} \to b\bar{b}g$ process the dominant contribution comes from the QHC amplitude, since the QHNC piece is additionally mass-suppressed. Here we consider two types of radiative background process that can mimic the $H \to b\bar{b}$ central exclusive signal.

(a) The extra gluon may go unobserved in the direction of one of the forward protons. This background may be reduced by requiring the approximate equality $M_{\rm missing} = M_{b\bar{b}}$. But the degree of this reduction will depend on the mass resolution in the proton detector and jet energy resolution in the central detector. Since the mass (jet energy) resolution $\Delta M_{b\bar{b}}$ in the central detector is expected to be much worse than the missing mass resolution, $\Delta M_{\rm missing} \ll \Delta M_{b\bar{b}}$, the background will be limited in practice by the $\Delta M_{b\bar{b}}$ value.
(b) The remaining danger is large-angle hard gluon emission which is collinear with either the b or $\bar{b}$ jet, and, therefore, unobservable. As discussed in [14, 39], for $J_z = 0$ this is suppressed for *soft* gluon radiation. Although there is a certain suppression of collinear radiation as well, this issue requires further detailed analysis, see below.
According to the study in [14], if the cone angle needed to separate the g jet from the b (or $\bar{b}$) jet is $\Delta R \sim 0.5$ then the expected background from unresolved three jet events leads to $B/S \simeq 0.2$. The calculations presented in Sect. 3 below will allow a more precise evaluation of this ratio.
It is worth noting that a detailed experimental study of the three-jet $b\bar{b}g$ final state could be useful for background calibration purposes. This is of particular interest for the kinematic configurations which are enhanced, for example when an energetic gluon recoils against a quasi-collinear $b\bar{b}$ pair. Recall also that the CDF collaboration is currently measuring exclusive $b\bar{b}$ production at the Tevatron [47, 48].

Note that in this paper we do not discuss the effects coming from collisions of *two* soft Pomerons, neither do we address a possible contribution from central inelastic production, see [13]. The reduction of such backgrounds is controlled by imposing the missing mass equality, see [14]. Note also that gluon radiation off the screening gluon (labelled 'Q' in Fig. 1) is numerically small [49].

2.2 Properties of the leading-order $gg^{\rm PP} \to b\bar{b}$ background process

As we have discussed, an important advantage of the $p + (H \to b\bar{b}) + p$ signal is that there exists a $J_z = 0$ selection rule, which requires the LO $gg^{\rm PP} \to b\bar{b}$ background to vanish in the limit of massless quarks and forward outgoing protons. However, in practice, LO background contributions remain, see [14]. The prolific $gg^{\rm PP} \to gg$ subprocess can mimic $b\bar{b}$ production when the outgoing glu-

[4] Although a number of automated packages are available for tree-level scattering amplitudes for arbitrary final states, it is very difficult to extract from these the projection onto a specific spin (e.g. $J_z = 0$) and colour (e.g. colour singlet) initial state.

ons are misidentified as b and $\bar{b}$ jets. Assuming the expected 1% probability of misidentification, and applying a $60^\circ < \theta < 120^\circ$ jet cut, gives a background-to-signal ratio $B/S \sim 0.2$ [14, 18, 19]. (Here and in what follows, we assume for reference that the mass window over which we collect the signal is $\Delta M \sim 3\sigma = 3\,\mathrm{GeV}$)[5].

Secondly, there is an admixture of $|J_z| = 2$ production, arising from non-forward going protons, which gives $B/S \sim 0.05$, see Sect. 2.5[6].

Thirdly, in reality the quarks have non-zero mass and there is a contribution to the $J_z = 0$ cross section of order m_b^2/E_{T}^2, where E_{T} is the transverse energy of the b and $\bar{b}$ jets. In [14, 18, 19] the contribution from this source was estimated as $B/S \sim 0.2$. However the higher-order QCD effects may strongly affect this result. First, there is a reduction coming from the self-energy insertion into the b-quark propagator, that is from the running of the b-quark mass from $\overline{m}_b(m_b)$ to its value $\overline{m}_b(M_{\mathrm{H}}) < \overline{m}_b(m_b)$ at the Higgs scale. Here $\overline{m}_b(\mu)$ is the running b-quark mass in the $\overline{\mathrm{MS}}$ scheme [50]. It is known that in the $H \to b\bar{b}$ decay width these single logarithmic (SL) ($\alpha_{\mathrm{S}} \ln \frac{M_{\mathrm{H}}}{m_b}$) effects diminish the corresponding Born result by a factor of approximately two [51–55]. Although this still requires a more formal proof, we strongly believe that the same (factor of two) reduction applies in the case of mass-suppressed $J_z = 0$ binary reactions $gg^{\mathrm{PP}} \to b\bar{b}$ and $\gamma\gamma \to b\bar{b}$ at large angles.

There is another (potentially important) source of uncertainties in the evaluation of the rate of exclusive $b\bar{b}$ production at $J_z = 0$. This is related to the so-called non-Sudakov form factor in the cross section F_q which arises from virtual diagrams with gluon exchange between the final quarks (or initial gluons), see [40, 56–60]. In the $\gamma\gamma$ case the double logarithmic (DL) approximation to F_q has the form

$$F_q(L_m) = \sum_n c_n \left(\frac{\alpha_{\mathrm{S}}}{\pi} L_m^2\right)^n \tag{4}$$

with

$$L_m \equiv \ln\left(\frac{M_{\mathrm{H}}}{m_b}\right), \tag{5}$$

$c_0 = 1$ and $c_1 = -8$ [56] so that the second (negative) term in (4) is anomalously large and dominates over the Born term for $M_{\mathrm{H}} \sim 100\,\mathrm{GeV}$. This dominance undermines the results of any analysis based on the one-loop approximation. The physical origin of this non-Sudakov form factor was elucidated in [40] where its explicit calculation in the two-loop approximation was performed. It was also shown that for reliable calculations of the DL effects the two-loop calculation should be sufficient. This was subsequently confirmed by a more comprehensive all-orders study [57–60]. As is well known, there are other DL effects (the so-called Sudakov logarithms [61]) that arise from virtual soft gluon exchanges. Their contribution depends on the particular kinematics in the final state. As discussed in [40], in the case of quasi-two-jet configurations Sudakov and non-Sudakov effects can be with good accuracy factorised, because they correspond to very different virtualities of the internal quark and gluon lines. For the final state radiation, the Sudakov effects (both for the signal and for the background) can be implemented in parton shower Monte Carlo models in a standard way. For the gg^{PP} initial state, the Sudakov factors are explicitly incorporated in the unintegrated gluon densities, see [13, 23]. Currently, for Higgs production at the PC the DL factors are accounted for by the simulation programme used for generating background events, see [44]. Unfortunately, from a phenomenological perspective, it seems to be potentially dangerous to rely on the DL results, since experience shows that formally subleading SL corrections may be numerically important. We plan to address this issue in future.

Nevertheless, as a first step in understanding the situation in the pp case it is instructive to evaluate the size of the DL effects for the $gg^{\mathrm{PP}} \to b\bar{b}g$ reaction. Recall that in the photon–photon case the two-loop expression for F_q takes the form [40]

$$F_q = (1 - 3\mathcal{F})^2 + \frac{\mathcal{F}^2}{3}\left(1 + \frac{C_A}{C_F}\right), \tag{6}$$

with[7]

$$\mathcal{F} = \frac{\alpha_{\mathrm{S}}}{\pi} C_F L_m^2 . \tag{7}$$

The corresponding one-loop result for the gg^{PP} initiated process is

$$F_g = 1 - (2C_F + 4N_c)\mathcal{F}/C_F \sim (1 - (C_F + 2N_c)\mathcal{F}/C_F)^2 . \tag{8}$$

Unfortunately, due to the large colour coefficients the one-loop DL contribution becomes larger than the Born term, and the final result will be strongly dependent on the NNLO contribution as well as on the scale μ at which the QCD coupling α_{S} is evaluated and on the running b-quark mass. It seems plausible to choose the scale $\mu \sim M_{\mathrm{H}}/2$ (since we are interested in the $b\bar{b}$ background at $s = M_{b\bar{b}}^2 = M_{\mathrm{H}}^2$) for the Born amplitude, but a lower scale $\mu \sim \sqrt{M_{\mathrm{H}} m_b}$ for the factor $\mathcal{F}$ in (7) which originates in the region where the quark propagators are close to the mass-shell. The NLL can be effectively incorporated in (6) and (8) by introducing a scale factor c in the argument of the logarithm, that is by replacing the ratio M_{H}/m_b by cM_{H}/m_b. It follows from the comparison with the complete one-loop calculation [56] for the process $\gamma\gamma(J_z = 0) \to b\bar{b}$,

[5] Such a background is practically negligible in the case of the PC since it must be mediated by the higher-order 'box' diagrams.

[6] Analogous to this in the PC case is the contribution from the initial photon state with $|J_z| = 2$, which may constitute a non-negligible source of background.

[7] Note that an additional problem is that while in the Born cross section it is natural to evaluate α_{S} at the hard scale M_{H}, for $\mathcal{F}$ we have no reason to adopt this prescription. The existing PC generators do not take into account possible differences in the scale of α_{S} for the different quantities.

that the scale factor $c \simeq 0.5$. This looks quite reasonable if we account for the kinematical configuration.

Without the complete result for the higher-order radiative corrections corresponding to the $gg^{\rm PP} \to b\bar{b}$ amplitude, it is impossible to make a firm prediction. To gain an insight into the size of the possible effects, we make the assumption that the same scale factor $c = 1/2$ is valid in this case as well. Then choosing $\alpha_{\rm S} = \alpha_{\rm S}(M_{\rm H} m_b) \sim 0.15$, the value of the correction $(1 + 2N_c/C_F)\mathcal{F} \simeq 2.5$ exceeds the Born term. In other words, the whole amplitude changes sign and the background cross section becomes a few times larger than the Born expectation.

Accounting for the running b-quark mass, the expected non-Sudakov correction factor can be approximated by

$$\left[1 - \frac{m_b(M_{\rm H} m_b)}{m_b(M_{\rm H}^2)}(C_F + 2N_c)\frac{\alpha_s(M_{\rm H} m_b)}{\pi}\ln^2 \times \left(\frac{cM_{\rm H}}{m_b(M_{\rm H} m_b)}\right)\right]^2 . \tag{9}$$

For the $\gamma\gamma$ case we have a similar expression

$$\left[1 - \frac{m_b(M_{\rm H} m_b)}{m_b\,(M_{\rm H}^2)} 3C_F \frac{\alpha_s(M_{\rm H} m_b)}{\pi}\ln^2\left(\frac{cM_{\rm H}}{m_b(M_{\rm H} m_b)}\right)\right]^2 . \tag{10}$$

If we take these formulae literally we would conclude that in the gg case the quasi-two jet cross section is a factor of 2 larger than the 'naive' (but frequently used) Born prediction, calculated with $\alpha_{\rm S}(M_{\rm H})$ and the b-quark pole mass. Similarly, for the $\gamma\gamma$ process the result is about 5 times lower than such a naive Born estimate.

While for the $\gamma\gamma$ case the estimated effect seems to be reasonably justified, for the gluon-initiated process it can serve only as a rough illustration of the possible size of the effect. The actual results will depend crucially on the value of the scale factor c (i.e. the NLL contributions) and on the specific choice of the arguments of the running coupling $\alpha_{\rm S}$ and b-quark mass. The main purpose of the exercise was to demonstrate that, currently (or, at least, before a complete one-loop result becomes available), the $gg^{\rm PP} \to b\bar{b}$ cross section can be estimated to no better than an order of magnitude accuracy.

2.3 Quasi-two-jet-like radiative background events

As was first found in [56] for the $\gamma\gamma$ case, there is an additional NNLO contribution which is not mass-suppressed and is potentially important especially for large energies. It comes from the QHC box diagrams. This piece cannot be evaluated in terms of the tree-level amplitudes using the cutting rules in 4 dimensions. A systematic method for calculating such amplitudes in the massless limit is based on generalised unitarity in D-dimensions, see for instance [62, 63]. An explicit calculation in [56] using dimensional regularization of the NNLO process $\gamma\gamma \to q\bar{q}$ at large angle θ gives

$$\frac{{\rm d}\sigma^{\rm NNLO}}{{\rm d}\sigma_{\rm Born}}(\gamma\gamma \to q\bar{q}, J_z = 0) = \frac{\alpha_{\rm S}^2}{32} C_F^2 \frac{s}{m_b^2}\cos^2\theta(1 - \cos^2\theta)\,, \tag{11}$$

with

$$\frac{{\rm d}\sigma_{\rm Born}}{{\rm d}\cos\theta}(\gamma\gamma \to q\bar{q}, J_z = 0) = \frac{12\pi\alpha^2 Q_q^4}{s}\frac{\beta(1-\beta^4)}{(1-\beta^2\cos^2\theta)^2}\,, \tag{12}$$

where $\beta \equiv \sqrt{1 - 4m_q^2/s}$, and m_q and Q_q are the mass and electric charge of the quark respectively[8]. Note that as is easily seen from (12), the NNLO elastic cross section vanishes at $\theta = \pi/2$. This is a consequence of the rotational invariance about the quark direction at 180° and the identity of the photons (see [39]) and remains valid in the absence of radiation at all orders in $\alpha_{\rm S}$. This is also true for the $gg^{\rm PP} \to q\bar{q}$ process. The ratio in (12) reaches its maximum at $\theta = \pi/4$ where

$$\frac{{\rm d}\sigma^{\rm NNLO}}{{\rm d}\sigma_{\rm Born}}(\gamma\gamma \to q\bar{q}, J_z = 0) = \frac{\alpha_s^2}{72\pi^2}\frac{s}{m_b^2}\,. \tag{13}$$

Accounting for the running b-quark mass and the NLLO effects discussed in the previous Section, we conclude that even at $M_{\rm H} \simeq 140\,{\rm GeV}$ these NNLO contribution to the cross section could not exceed 0.1 of the modified Born term. The NNLO elastic $c\bar{c}$ contribution is 16 times larger, and at $M_{\rm H} \simeq 130\,{\rm GeV}$ becomes comparable with the modified $b\bar{b}$ exclusive term. However with a reasonably good experimental c-quark rejection this background can be strongly reduced without seriously degrading the $H \to b\bar{b}$ signal.

Using the existing results for the one-loop amplitudes of the $gg \to b\bar{b}$ process in the massless limit (see for example [64–66]) we can write down the corresponding NNLO expression for the ratio of the $gg^{\rm PP} \to b\bar{b}$ subprocesses as

$$\frac{{\rm d}\sigma^{\rm NNLO}}{{\rm d}\sigma_{\rm Born}}(gg^{\rm PP} \to q\bar{q}, J_z = 0) = \frac{(C_F - N_c)^2}{C_F^2}\frac{{\rm d}\sigma^{\rm NNLO}}{{\rm d}\sigma_{\rm Born}} \times (\gamma\gamma \to q\bar{q}, J_z = 0)\,. \tag{14}$$

Note that the appearance of the $(C_F - N_c)^2$ factor in (14) is not accidental. It is a consequence of supersymmetry requiring the vanishing of such helicity amplitudes in a supersymmetric theory, which happens if we put the fermions in the adjoint representation (gluinos)[9]. This is in marked contrast with the combination $(C_F + 2N_c)^2$ that appears in (8), where the result is of a purely classical nature and supersymmery arguments cannot be applied. Note that in the massive quark case, even if we were to consider altering its colour representation from the fundamental to the adjoint representation, we cannot put it into the same supersymmetric multiplet with the massless gluon [67].

[8] In [40] there are some confusing statements regarding the properties of the $\gamma\gamma \to b\bar{b}$ amplitude in the complex plane and the interpretation of the one-loop amplitude result of [56]. But these do not affect the actual formulae.

[9] We are grateful to Lance Dixon for an illuminating discussion of the properties of helicity amplitudes in a supersymmetric theory.

2.4 Admixture of $|J_z| = 2$ production, arising from non-forward going protons

In the exact forward direction, the $J_z = 0$ selection rule is just a consequence of the s-channel helicity conservation for the forward protons. For the non-zero transverse momenta of the outgoing protons $(p_{1,t}, p_{2,t})$ some admixture of the $|J_z| = 2$ component appears. Its value is controlled by the orbital momentum transfered through the Pomeron (i.e. through the colour singlet t-channel two gluon exchange) that is by the product $(p_{t,i} r_t)$, where $i = 1, 2$, and the effective Pomeron size $r_t \simeq 1/Q_t$ is driven by the inverse transverse momentum Q_t in the gluon loop. Thus, this admixture of the $|J_z| = 2$ states can be evaluated as [28, 29] $2p_{1,t}p_{2,t}/Q_t^2$ in the amplitude or

$$\frac{(2p_{1,t}p_{2,t})^2}{Q_t^4} \tag{15}$$

for the cross section. An additional factor 2 arises from the azimuthal angular averaging $(Q_j Q_k \to \delta^{(2)}_{j,k} Q_t^2/2)$.

Technically the polarisation structure is as follows. In the equivalent gluon approximation the polarisation vector of the active gluon is proportional to its transverse momentum $e_{\mu,i} \simeq (p_{t,i} - (-1)^i Q_t)_\mu / x_i$ $(i = 1, 2)$[10]. Thus the product of two polarisation vectors can be written as

$$e_{\mu,1}e_{\nu,2} = \frac{(p_{t,1} - Q_t)_\mu (p_{t,2} + Q_t)_\nu}{x_1 x_2}\,,$$
$$e_{\mu,1}e_{\nu,2} \propto\ p_{t,1,\mu}p_{t,2,\nu} - Q_{t,\mu}Q_{t,\nu} + (Q_{t,\mu}p_{t,2,\nu} - p_{t,1,\mu}Q_{t,\nu}). \tag{16}$$

After the $(\mathbf{Q}_t)$ angular integration the last term in (16) vanishes while the second term gives $-\delta^{(2)}_{\mu\nu} Q_t^2/2$. In terms of helicity amplitudes, $\delta^{(2)}_{\mu\nu}$ corresponds to a pure $J_z = 0$ state. On the other hand, the first term in (16), after the averaging over $p_{t,i}$ directions, generates the $J_z = 0$ and $|J_z| = 2$ states with equal probabilities. Unfortunately, the amplitude with an extra $1/Q_t^2$ factor becomes less convergent at small Q_t^2. The dominant contribution comes from the region of relatively low $Q_t \sim$ GeV (and even lower for the Tevatron energies). Therefore, we cannot guarantee the precision of the numerical evaluation. Using the MRST99 partons [68] we expect the $|J_z| = 2$ admixture for central exclusive production of the state with the mass $M \sim 120 - 160$ GeV to be about 5% at Tevatron energies and $\sim 1.5\%$ at the LHC ($\sqrt{s} = 14$ TeV) [28, 29].

There is good news however. It is worth noting that the $|J_z| = 2$ contribution to the $gg^{\rm PP} \to q\bar{q}$ background is additionally suppressed numerically (by a factor of, at least, ~ 0.2)[11]. In order to gain an insight into the origin of this additional suppression, we note that the cross section vanishes at $\theta = \pi/2$ in the $q\bar{q}$ rest frame (neglecting the proton transverse momenta in comparison with the transverse energy of the quarks). This follows from the identity of the incoming gluons (protons) and invariance with respect to the 180° rotation about the quark direction. This in turn, causes the cross section to be proportional to $\cos^2\theta$. This phenomenon is also seen in the vanishing of the NNLO non-radiative amplitude at $\theta = \pi/2$ considered in Sect. 2.3, and in the soft radiation off the screening gluon, considered in [49] (see also the discussion in [39]).

2.5 NLO radiation close to the beam directions

The NLO subprocess $gg^{\rm PP} \to b\bar{b}g$ can also avoid the $J_z = 0$ selection rule. Extra gluon radiation in the beam direction goes into the beam pipe, and cannot be observed directly. Therefore, experimentally, the event may look like central exclusive production. There are two main consequences of this extra gluon radiation: a) the system M_8 which is centrally produced via $gg \to M_8$ fusion is now in the colour octet state (which we label by the symbol '8'), and (b) the $J_z = 0$ selection rule, which suppresses the $b\bar{b}$ LO QCD production in the genuine central exclusive event, becomes redundant.

Let us discuss this point in more detail. The emission of a low q_t extra gluon is strongly suppressed due to the distructive interference between the amplitudes where the gluon q_μ is emitted from the right (active) or from the left (screening) t-channel gluons in Fig. 1. Therefore, it is sufficient to consider the case when $M_{\rm H} \gg q_t \gg Q_t$, and the polarisation of the active gluon (participating in the $gg \to M_8$ fusion process) is directed along the new vector $\mathbf{q}_t$. Assuming that the extra gluon with momentum q_μ is emitted from the lower active gluon $(i = 2)$, the polarisation structure becomes

$$e_{\mu,1}e_{\nu,2} \propto\ (p_{t,1,\mu} - Q_{t,\mu})(q_{t,\nu} + Q_{t,\nu}) \simeq p_{t,1,\mu}q_{t,\nu} - Q_{t,\mu}q_{t,\nu} - \delta^{(2)}_{\mu\nu} Q_t^2/2\,, \tag{17}$$

where the last term corresponds to the $J_z = 0$ state and the first term corresponds to the hard subprocess, which after the $\mathbf{q}_t$ and $\mathbf{p}_{t,1}$ averaging looks like the usual fusion of two unpolarised gluons (with equal probabilities for the $J_z = 0$ and $|J_z| = 2$ initial states). The contribution generated by the second term is more complicated. At first sight it should vanish after the integration over the azimuthal $\mathbf{Q}_t$ angle, however due to the factor $(\mathbf{Q}_t + \mathbf{q}_t)^2$ in the denominator of the amplitude some component of the momentum $Q_{t,\mu}$ in the $q_{t,\mu}$ direction still survives. In the limit of $q_t \gg Q_t$ this leads to a contribution $\sim q_{t,\mu}q_{t,\nu}Q_t^2/q_t^2$ to the right-hand side of (17), which again contains the $J_z = 0$ and $|J_z| = 2$ states with equal probabilities.

Thus, the ratio of the $|J_z| = 2$ to $J_z = 0$ contributions to the cross section for this process may be evaluated as

$$\frac{\sigma(|J_z| = 2)}{\sigma(J_z = 0)} = \frac{< Q_t^2 >^2 + < p_t^2 >< q_t^2 >}{2 < Q_t^2 >^2 + < p_t^2 >< q_t^2 >}\,. \tag{18}$$

[10] Alternatively, the same result can be obtained in the LO using the planar gauge $(n_\mu A^a_\mu) = 0$ with the gauge 4-vector n_μ parallel to the 4-momentum of the centrally produced system M.

[11] This suppression was not accounted for in [14, 28, 29]. This provides added value to the improvement of the signal-to-background situation in the $b\bar{b}$-case.

We might expect that the probability to emit such an extra gluon would contain a double logarithm, but this does not happen. First, as will be discussed in Sect. 4, for the massless b-quark case the soft gluon emission $gg^{\rm PP} \to b\bar{b}g$ is suppressed by a factor $(E_{\rm g}/M_{b\bar{b}})^4$ and therefore gives no logarithm. On the other hand, the collinear logarithm is limited by the angular acceptance of the detector. Any gluon with a sufficiently large q_t will be observed in the Central Detector. Moreover, up to pseudorapidities $|\eta| \sim$ 6–7 the extra gluon jet will be observed experimentally in a forward detector. Such events with a third jet will be easily distinguished from the $H \to b\bar{b}$ decay. Next, if the energy of the gluon q exceeds the mass resolution then there will be no matching between the missing mass calculated from the momenta of the outgoing forward protons and the mass M_8 measured in the Central Detector. Assuming the mass resolution $\Delta M_{b\bar{b}} \sim 20\,\text{GeV}$, we require that for central $b\bar{b}$ production the energy of the third (forward) gluon jet must be less than 40 GeV, and to get $|\eta| > 6$ such a jet must have a very small transverse momentun, $q_t < 2E_{\rm g}\exp(-6) = 0.2\,\text{GeV}$. The production of such a low $q_t (\ll Q_t)$ gluon is strongly suppressed by the interference between the emissions of the active gluon q_t and the screening gluon Q (see Fig. 1). This contribution becomes smaller than the admixture of the $|J_z| = 2$ states.

3 The $gg, \gamma\gamma \to q\bar{q}g$ $\quad |J_z| = 0$ colour singlet hard process

In this section we will present results for the matrix elements squared for the colour singlet hard scattering processes $gg \to q\bar{q}g$ and $\gamma\gamma \to q\bar{q}g$. Since we will be using these results in situations where the momentum transferred in the hard scattering is much larger than the b-quark mass, we will set $m_q = 0$. We will compare our results with the corresponding full spin- and colour-summed amplitudes in order to exhibit the different limiting behaviours.

In fact the spin- and colour-summed matrix element squared for the $2 \to 3$ process $g(p_1) + g(p_2) \to g(p_3)q(p_4)\bar{q}(p_5)$ process has been known for a long time [69] and has a relatively simple analytic form:

$$\begin{aligned}\sum |\mathcal{M}|^2 &= \frac{g_s^6}{4N^2(N^2-1)} \\ &\times \left(\frac{a_1b_1\left(a_1^2+b_1^2\right)+a_2b_2\left(a_2^2+b_2^2\right)+a_3b_3\left(a_3^2+b_3^2\right)}{a_1a_2a_3b_1b_2b_3}\right) \\ &\times \left[\frac{s}{2}+N^2\left(\frac{s}{2}-\frac{a_1b_2+a_2b_1}{d_{12}}-\frac{a_2b_3+a_3b_2}{d_{23}}-\frac{a_3b_1+a_1b_3}{d_{13}}\right)\right. \\ &+\frac{2N^4}{s}\left(\frac{a_3b_3(a_1b_2+a_2b_1)}{d_{23}d_{13}}+\frac{a_1b_1(a_2b_3+a_3b_2)}{d_{12}d_{13}}\right. \\ &\left.\left.+\frac{a_2b_2(a_3b_1+a_1b_3)}{d_{12}d_{23}}\right)\right], \end{aligned} \tag{19}$$

where $a_i = p_ip_4,\ b_i = p_ip_5,\ d_{ij} = p_ip_j\ \ (i,j = 1,\ldots 3)$ and $s = 2p_4p_5$. An averaging over initial spins $(1/4)$ and colours $(1/(N^2-1)^2 = 1/64)$ has been performed. In fact the above spin-summed amplitude squared comprises 12 distinct non-zero helicity combinations, 4 of which

$$(++;--+)\,,(++;-+-)\,,(--;+-+)\,,(--;++-) \tag{20}$$

(in an obvious notation) correspond to a $J_z = 0$ initial state, while the remaining 8

$$\begin{aligned}&(-+;+-+)\,,(-+;--+)\,,(-+;++-)\,,(-+;-+-)\,,\\ &(+-;+-+)\,,(+-;--+)\,,(+-;++-)\,,(+-;-+-)\end{aligned} \tag{21}$$

correspond to a $|J_z| = 2$ initial state. Note that in all cases $\lambda_q = -\lambda_{\bar{q}}$, corresponding to helicity conservation along the fermion line. The other important point to note is that all the above combinations are MHV amplitudes [41, 42], in the sense that the sum of the (five) helicities is always ± 1. At this order there are no NMHV amplitudes or higher. MHV $gggq\bar{q}$ scattering amplitudes have a very simple analytic form, see the Appendix, and so with appropriate colour weightings and momentum permutations, the colour singlet $J_z = 0, \pm 2$ matrix elements squared can be easily constructed. The result is

$$\begin{aligned}\sum |\mathcal{M}|^2(J_z = 0;\ \text{colour singlet}\ ) &= \frac{2}{9}\sum_{h=1}^{4}\Big|z(1,2,3,h) \\ &+ z(2,1,3,h) + z(3,2,1,h) + z(3,1,2,h) \\ &- \frac{1}{8}\left(z(1,3,2,h) + z(2,3,1,h)\right)\Big|^2 \end{aligned} \tag{22}$$

where spin and colour averaging factors are included. The z factors are given in the Appendix. Expressions for the other spin and colour combinations can also be written down in terms of the $z(i,j,k,h)$ factors. However these are more lengthy and so will not be presented here.

Compact analytic expressions exist for the corresponding $\gamma\gamma \to gq\bar{q}$ spin summed and $J_z = 0$ amplitudes squared. In the notation of (19),

$$\begin{aligned}\sum |\mathcal{M}|^2_{\gamma\gamma}(\ \text{spin summed}\ ) &= 8g_s^2e^4\frac{s}{2} \\ &\times \left(\frac{a_1b_1\left(a_1^2+b_1^2\right)+a_2b_2\left(a_2^2+b_2^2\right)+a_3b_3\left(a_3^2+b_3^2\right)}{a_1a_2a_3b_1b_2b_3}\right), \\ \sum |\mathcal{M}|^2_{\gamma\gamma}(J_z = 0) &= 8g_s^2e^4\frac{s}{2}\left(\frac{a_3^2+b_3^2}{a_1a_2b_1b_2}\right). \end{aligned} \tag{23}$$

4 Numerical results and discussion

In this section we consider some of the properties of the amplitudes presented in the previous section and, in particular, focus on the differences between the spin-summed (unpolarised) and $J_z = 0$ cases. The differences are most dramatic for the kinematic configuration in which the final-state gluon is *soft*. It follows from the $E_{\rm g} \to 0$ limit of (23) that the matrix element squared for the $J_z = 0$ case is proportional to E_g^2, while in the unpolarised case it exhibits

the standard $1/E_g^2$ behaviour. This is because the first two terms in the bracket on the right hand side in the unpolarised case, which are responsible for the leading infrared behaviour in the soft-gluon limit, are absent in the $J_z = 0$ case. The net difference is four powers of a_3 or b_3, equivalently $E_{\rm g}^4$. Numerical calculation shows that exactly the same behaviour is found in the gg scattering cases.

In terms of the cross sections in the soft gluon limit,

$$\frac{{\rm d}\sigma(J_z=0)}{{\rm d}E_{\rm g}} \sim E_g^3\,, \tag{24}$$

while in the unpolarised case we arrive at the the standard infrared behaviour

$$\frac{{\rm d}\sigma_{\rm unpol}}{{\rm d}E_{\rm g}} \sim \frac{1}{E_{\rm g}}\,. \tag{25}$$

Such behaviour is rooted in the Low–Burnett–Kroll (LBK) [70, 71] theorem (see also [39, 72, 73]). According to the LBK theorem, for radiation of a soft gluon with energy fraction $x_{\rm g} \ll 1$, the radiative matrix element $M_{\rm rad}$ may be expanded in powers of the scaled gluon energy $x_{\rm g} = E_{\rm g}/E_b$

$$M_{\rm rad} \sim \frac{1}{x_{\rm g}} \sum_{n=0}^{\infty} C_n x_{\rm g}^n\,, \tag{26}$$

where the first two terms, with coefficients C_0 and C_1 (which correspond to long-distance radiation), can be written in terms of the non-radiative matrix element M_B. The application of these classical results is especially transparent when the cross sections are integrated over the azimuthal angles. Then the non-radiative process depends only on simple variables, such as the centre-of-mass energy. When $M_B = 0$, the expansion starts from the non-universal $C_2 x_{\rm g}^2$ term, which corresponds to non-classical (short-distance) effects, not related to M_B. This is exactly the case for the $J_z = 0$ Born amplitudes which vanish for massless quarks for both $\gamma\gamma$ and $gg^{\rm PP}$ processes[12]. On the other hand, in the soft limit the unpolarised result is dominated by the non-vanishing non-radiative amplitudes, either $(-+;+-)$, $(-+;-+)$ or $(+-;+-)$, $(+-;-+)$, and in this case the matrix element squared, $|M_{\rm rad}|^2$, is proportional to $1/E_g^2$. Recall, however, that the mass-suppressed contributions to the $J_z = 0$ amplitudes will induce the normal infrared behaviour, see for example [39], i.e.

$$\frac{{\rm d}\sigma(J_z=0)}{{\rm d}E_{\rm g}} \sim \frac{m_b^2}{s}\frac{1}{E_{\rm g}}\,. \tag{27}$$

Note that here and in what follows $s = (p_1+p_2)^2$ is the invariant mass squared of the 3-jet system. The above behaviour is illustrated in Fig. 2 where we plot[13] the matrix elements squared as a function of the scaled gluon energy

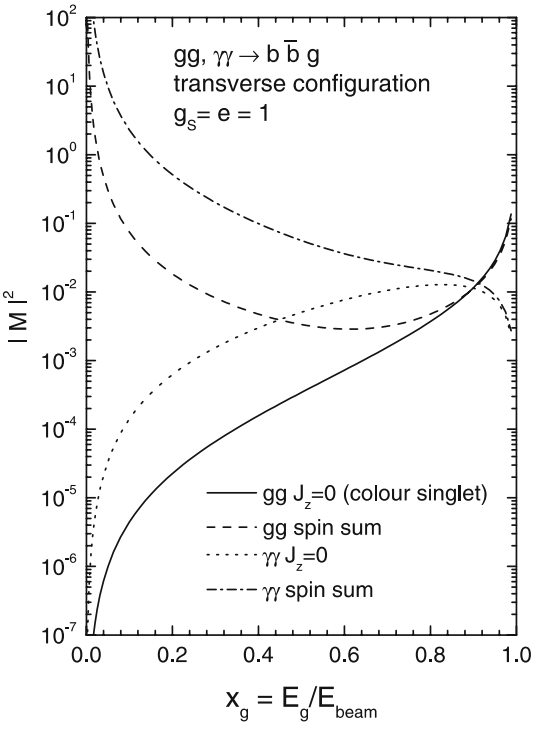

Fig. 2. Dependence of the $gg, \gamma\gamma \to b\bar{b}g$ matrix element squared on the final-state gluon fractional energy, when all three particles are produced in the transverse plane and the b and $\bar{b}$ have equal energy. Note that the b-quark mass is set to zero

$x_{\rm g} = E_{\rm g}/E_{\rm beam}$. For simplicity, we work in the centre-of-mass frame with all final state particles in the transverse plane and equal energies for the (massless) quark and antiquark. In this configuration, $x_{\rm g} \to 0$ is the soft gluon limit, $x_{\rm g} = 2/3$ is the (transverse) 'Mercedes' configuration, and $x_{\rm g} \to 1$ corresponds to a transverse gluon balanced by a collinear $q\bar{q}$ pair.

The expected LBK behaviour discussed above ($x_{\rm g}^2$ versus $x_{\rm g}^{-2}$) is clearly seen in the $x_{\rm g} \to 0$ limit. Note also that the gg (but not the $\gamma\gamma$) amplitudes become singular as $x_{\rm g}$ approaches the kinematic limit at $x_{\rm g} = 1$. This is the collinear singularity caused by the production of two final-state back-to-back gluons, one of which splits into a quark-antiquark pair, i.e. $g \to q\bar{q}$. For these kinematics, this is manifest as a $(1-x_{\rm g})^{-1}$ singularity in the matrix elements squared. There is no analogue in the $\gamma\gamma$ case, and indeed here the amplitudes vanish in the $x_{\rm g} \to 1$ limit. since at $x_{\rm g} \to 1$ the quark and antiquark go in exactly the same direction and their electric charges screen each other. Thus the coupling of the photon to the $q\bar{q}$ pair vanishes.

More generally, we can study the behaviour of the matrix elements squared when all three particles lie in the transverse plane by using the Dalitz-plot variables x_q and $x_{\bar{q}}$, the scaled energies of the final state quark and antiquark respectively, with $x_q + x_{\bar{q}} + x_{\rm g} = 2$. For the $J_z = 0$ $\gamma\gamma \to q\bar{q}g$ case, it is straightforward to show that

$$\sum |\mathcal{M}|^2_{\gamma\gamma}(J_z=0) = \frac{256 g_s^2 e^4}{s}\left[(1-x_q)^2 + (1-x_{\bar{q}})^2\right]$$

[12] Actually, the $J_z = 0$ non-radiative matrix element vanishes for *any* colour state of two gluons since it corresponds to a maximally helicity violating (MHV) situation, see for example [43].

[13] For display purposes, the QCD and QED couplings g_s and e are set to 1 in this plot.

$$\times \frac{x_q + x_{\bar{q}} - 1}{x_q^2 x_{\bar{q}}^2} \,. \tag{28}$$

In the limit where $x_{\bar{q}}$ (or x_q) $\to 1$, an antiquark balances a collinear quark–gluon pair, and the matrix element squared becomes

$$\sum |\mathcal{M}|^2_{\gamma\gamma}(J_z = 0) \to \frac{256 g_s^2 e^4}{s}(1-x)^2/x \,, \tag{29}$$

with $x = 1 - x_{\rm g}$ the fractional quark momentum of the quark–gluon pair. Note also that the matrix element squared vanishes when the quark and antiquark are emitted in the same direction ($x_q + x_{\bar{q}} = 1$), as anticipated above.

For the gg scattering case, there is no simple analogue of (28) for the whole Dalitz-plot. However, the behaviour along the boundaries can be extracted and studied. We find

$$\sum |\mathcal{M}|^2_{gg}(J_z = 0) = \frac{g_s^6}{s}\left[(1-x_q)^2 + (1-x_{\bar{q}})^2\right] \frac{F(x_q, x_{\bar{q}})}{x_q + x_{\bar{q}} - 1}, \tag{30}$$

where $F(x, y)$ is a non-singular function with constant values along the three sides of the Dalitz-plot:

$$\begin{aligned} F &= \frac{64}{9}, \quad \text{when } x = 1 \text{ or } y = 1 \\ F &= 36 \,, \quad \text{when } x + y = 1 \,. \end{aligned} \tag{31}$$

Note the jump of the function F at $x = 1, y \to 0$ and $y = 1, x \to 0$. These are the points where the soft antiquark (or quark) changes its direction, leading to a discontinuity in the classical coloured current.

To summarise, in the gg $J_z = 0$ colour-singlet case, the only final-state[14] singularity is when the gluon is emitted opposite a collinear quark–antiquark pair. In practical terms, this corresponds to the case when both b-quarks are contained within the same jet. Strictly speaking, this does not constitute a background to Higgs production, since the latter gives rise to two distinct b-jets.

In contrast, the full spin-, colour-summed gg amplitude has additional singularities when $x_q = 1$ or $x_{\bar{q}} = 1$. In fact the full singularity structure is exhibited in the empirical form

$$\sum |\mathcal{M}|^2_{gg}(\text{spin, colour summed}) = \frac{g_s^6}{s} \frac{G(x, y)}{(1-x_q)(1-x_{\bar{q}})(x_q + x_{\bar{q}} - 1)} \,, \tag{32}$$

where G is non-singular throughout the Dalitz-plot. Note that when $x_q = x_{\bar{q}} = 1 - x_{\rm g}/2$ – the kinematics of Fig. 2 – this reduces to

$$\sum |\mathcal{M}|^2_{gg}(\text{spin, colour summed}) = \frac{4 g_s^6}{s} \frac{G(1 - x_{\rm g}/2, 1 - x_{\rm g}/2)}{x_{\rm g}^2 (1 - x_{\rm g})} \,. \tag{33}$$

What does this mean for jet cross sections? Recall that in $e^+e^- \to q\bar{q}g$ the 'three-jet cross section' is defined by integrating the matrix element squared over a region away from the boundaries of the Dalitz-plot, the exact region depending on the jet algorithm definition. For example, the $y_{\rm cut}$ (JADE) algorithm defines the three-jet region by

$$1 - x_q, 1 - x_{\bar{q}}, x_q + x_{\bar{q}} + 1 > y_{\rm cut} \,. \tag{34}$$

Given the absence of collinear singularities in the $J_z = 0$, colour-singlet case when the gluon is emitted parallel to the quark or antiquark, we may therefore expect relatively more radiative three-jet events than in the $|J_z| = 2$ or spin-summed cases. Note, however, that the three jet cross section is still (logarithmically) singular in the $y_{\rm cut} \to 0$ limit corresponding to the configuration $x_q + x_{\bar{q}} \to 1$ in which the final-state b and $\bar{b}$ are collinear, i.e. $g + g \to g + g^* (\to b\bar{b})$. However, such radiatively generated quasi-two-jet events can be suppressed by requiring two distinct, spatially-separated b-tagged jets. Indeed applying a minimum-angle cut between the b and $\bar{b}$ jets leads to a finite ($J_z = 0$, colour-singlet) three-jet cross section.

Note that in order to compare the matrix elements for the $\gamma\gamma \to b\bar{b}g$ and $gg \to b\bar{b}g$ reactions in Fig. 2 we set the couplings $g_s = e = 1$. Strictly speaking, at the leading order (tree level) at which we work, it is not known at what scale the couplings must be evaluated. However in actual cross section calculations it would appear natural to take two of the vertices at the large scale $\mu^2_{1,2} \sim s/2$ and the third (outgoing gluon emission) vertex at a lower scale $\mu_3^2 \sim k_\perp^2$, i.e. $|M|^2 \propto \alpha_s^2(s/2)\alpha_s(k_\perp^2)$, where $k_\perp$ is the transverse momentum of the final gluon with respect to the nearest (quark, antiquark or beam) jet direction.

In summary, provided that two distinct b-jets are required, then the dominant background arising from $gg \to b\bar{b}g$ production in the $J_z = 0$, colour-singlet case corresponds to three-jet production. The same is true for $\gamma\gamma$ production. Although we have concentrated our analysis on production in the transverse plane, this conclusion is still valid for central production, i.e. where the final state jets are restricted to a central region in rapidity.

5 Summary

In the previous sections we have shown (see also [39]) that, as a consequence of the Low–Burnett–Kroll theorem [70, 71], when neglecting the quark mass, the differential distribution over the gluon energy in the $\gamma\gamma, gg^{\rm PP} \to q\bar{q}g$ cross section is

$$\frac{{\rm d}\sigma(J_z = 0)}{{\rm d}E_{\rm g}} \sim E_g^3 \,, \tag{35}$$

in marked contrast to the Higgs or unpolarised case, where the cross sections exhibit the standard infrared behaviour

$$\frac{{\rm d}\sigma_{\rm unpol}}{{\rm d}E_{\rm g}} \sim \frac{1}{E_{\rm g}} \,. \tag{36}$$

[14] We note that we are considering here central production of all three final-state particles. There are of course additional singularities when the final-state gluon is emitted collinear with the incoming gluons, but these initial-state singularities are well understood.

As a result, the relative probability of the Mercedes-like configuration in the final $q\bar{q}g$ state for the $J_z = 0$ background processes becomes unusually large. We have derived explicit analytic expressions for the $\gamma\gamma, gg^{\rm PP} \to q\bar{q}g$ amplitudes using MHV techniques, and calculated some simple energy distributions to illustrate their generic behaviour. These amplitudes can easily be incorporated into more sophisticated Monte Carlo programmes to investigate background event rates in the presence of realistic experimental cuts.

Finally, the approach of [74] enables us to evaluate the difference between the charged multiplicities of the signal $N_{\rm S}$ and Mercedes-like background events $N_{\rm BG}^{\rm Merc}$ containing b-quarks for the $J_z = 0$ initial state for both processes $\gamma\gamma$ and $gg^{\rm PP}$ induced processes. As is shown in [74],

$$\Delta N = N_{\rm BG}^{\rm Merc}(M_{\rm H}) - N_{\rm S}(M_{\rm H}) = N_{q\bar{q}}\left(\frac{M_{\rm H}}{\sqrt{3}}\right) + \frac{1}{2}N_{gg}\left(\frac{M_{\rm H}}{\sqrt{3}}\right) - N_{q\bar{q}}(M_{\rm H})\,. \tag{37}$$

For example, for a 100 GeV Higgs boson, $2E_q^* = \frac{M_{\rm H}}{\sqrt{3}} \simeq 58$ GeV, which corresponds to the energies of the existing measurements by TOPAZ and VENUS, see [74]. Substituting into (37) the corresponding experimental results for $N_{q\bar{q}}$ and the fits to the gg multiplicity from [74], we arrive at the multiplicity difference between the Mercedes-like background events and the $b\bar{b}$ signal,

$$\Delta N = 6.8 \pm 1.5\,. \tag{38}$$

A similar result ($\Delta N \sim 8.0$) appears if we use the existing ($udscb$) direct data on the total charged multiplicity at the Z^0 pole and the corresponding number for the multiplicity of 3-jet events, see [74]. Note that the multiplicity difference rises as $M_{\rm H}$ increases. We expect that such a large effect could help to discriminate between the Higgs signal and background events containing b-quarks and in the analysis of the $b\bar{b}$ diffractive events at the Tevatron.

Acknowledgements. We thank Brian Cox, Albert De Roeck, Lance Dixon, Nigel Glover, Monika Grothe, Victor Fadin, Jeff Forshaw, Valya Khoze, Alan Martin, Klaus Moenig, Risto Orava, Andrei Shuvaev and Georg Weiglein for useful discussions. MGR thanks the IPPP at the University of Durham for hospitality. This work was supported by the UK Particle Physics and Astronomy Research Council, by a Royal Society special project grant with the FSU, by an INTAS grant 05-103-7515, by grant RFBR 04-02-16073 and by the Federal Programme of the Russian Ministry of Industry, Science and Technology SS-1124.2003.2.

Appendix: Helicity amplitudes for $gg \to gq\bar{q}$

Here we outline the formalism used to calculate the $gg \to gq\bar{q}$ scattering amplitude discussed in Sect. 3. We denote the colour indices of the incoming gluons by a, b, and of the outgoing gluon by c. The quarks colour indices are j, k.

The $gg \to gq\bar{q}$ matrix element, which depends on the helicities, h_i, and the 4-momenta, p_i, of the gluons and quarks, is given by the so-called dual expansion (see [43] and references therein)

$$M^{h_i}(p_i)_{jk} = \sum (\lambda_a\lambda_b\lambda_c)_{jk} z(a,b,c)\,, \tag{A.1}$$

where the sum is over the permutations of a, b, c. The first factor has the same structure as if all the gluons were emitted from the quark line. The λ_i are the standard matrices of the fundamental representation of SU(3), and are normalised as follows

$$\mathrm{Tr}(\lambda^a\lambda^b) = \frac{1}{2}\delta^{ab}\,, \tag{A.2}$$

$$[\lambda^a, \lambda^b] = if_{abc}\lambda^c\,. \tag{A.3}$$

The colour-ordered subamplitudes, $z(a,b,c,)$, are only functions of the kinematical variables of the process, i.e. the momenta and the helicities of the gluons. They may be written in terms of the products of the Dirac bispinors, that is in terms of the angular (and square) brackets

$$\langle ab\rangle = \langle p_a^- | p_b^+\rangle = \sqrt{|2p_ap_b|}e^{{\rm i}\phi_{ab}}\,, \tag{A.4}$$

$$[ab] = \langle p_a^+ | p_b^-\rangle = \sqrt{|2p_ap_b|}e^{{\rm i}\bar{\phi}_{ab}}\,, \tag{A.5}$$

where $2p_ap_b = s_{ab}$ is the square of the energy of the corresponding pair. If both 4-momenta have positive energy, the phase ϕ_{ab} is given by

$$\cos\phi_{ab} = \frac{p_a^x p_b^+ - p_b^x p_a^+}{\sqrt{p_a^+ p_b^+ s_{ab}}}\,, \quad \sin\phi_{ab} = \frac{p_a^y p_b^+ - p_b^y p_a^+}{\sqrt{p_a^+ p_b^+ s_{ab}}}\,, \tag{A.6}$$

with $p_i^+ = p_i^0 + p_i^z$, while the phase $\bar{\phi}_{ab}$ can be calculated using the identity $s_{ab} = \langle ab\rangle[ab]$.

Finally, the only non-zero $J_z = 0$ subamplitudes are

$$z(a,b,c;h) = ig_s^3 \frac{\langle qc\rangle\langle\bar{q}c\rangle\langle Ic\rangle^2}{\langle\bar{q}q\rangle\langle qa\rangle\langle ab\rangle\langle bc\rangle\langle c\bar{q}\rangle}\,. \tag{A.7}$$

Here g_s is the QCD coupling ($\alpha_s = g_s^2/4\pi$) and I denotes the quark (or antiquark) which has the same helicity as the outgoing gluon c. In particular, when $\lambda_a = \lambda_b = 1$ while $\lambda_c = \lambda_q$ ($\lambda_{\bar{q}} = -\lambda_q$) the numerator takes the form $\langle qc\rangle^3\langle\bar{q}c\rangle$. The expression (A.7) is written for the case of the incoming gluons with positive helicities. If we change the sign of all helicities, then we have simultaneously to replace the $\langle ij\rangle$ brackets by the $[ij]$ brackets.

Note that in the formalism leading to (A.7) all the gluons are considered as incoming particles; that is, the energies of gluon c and both quarks are negative. In the case when one or two momenta in the product $\langle ab\rangle$ have negative energy, the phase ϕ_{ab} is calculated with minus the momenta with negative energy, and then $n\pi/2$ is added to ϕ_{ab} where n is the number of negative momenta in the spinor product.

It is clear from (A.7) that in the limit of a soft outgoing gluon c the cross section obtains an extra factor $E_{\rm g}^4$ since the numerator of the amplitude

$$\langle qc\rangle\langle\bar{q}c\rangle\langle Ic\rangle^2 \propto E_{\rm g}^2\,. \tag{A.8}$$

This factor kills the soft gluon logarithm. The collinear logarithm corresponding to the kinematics where gluon c goes in, say, the quark q direction may come only from the subamplitudes $z(c,a,b;h)$ and $z(c,b,a;h)$ where the factor $\langle qc\rangle$ in the denominator of (A.7) provides the collinear singularity. However this singularity is cancelled by the analogous term in the numerator. Thus the most dangerous background configuration (where the gluon is very hard to separate from the quark jet) is not enhanced by any large logarithm.

It is straightforward to derive the analytical expression for the experimentally important kinematic configuration where the gluon and quark directions are aligned. This involved keeping just the two subamplitudes, $z(c,a,b;h)$ and $z(c,b,a;h)$, with the quark helicity opposite to the gluon c helicity (in order to have a larger numerator in (A.7)). This gives

$$\sum |\mathcal{M}|^2(J_z=0;\text{colour singlet}) = \frac{4g_s^6}{9}\frac{x_g^2 s}{E_T^4}\,. \quad \text{(A.9)}$$

References

1. LHC/LC Study Group Collaboration, G. Weiglein et al., arXiv:hep-ph/0410364
2. J.F. Gunion, H.E. Haber, R. Van Kooten, arXiv:hep-ph/0301023
3. ECFA/DESY Photon Collider Working Group Collaboration, B. Badelek et al., Int. J. Mod. Phys. A **19**, 5097 (2004) [arXiv:hep-ex/0108012]
4. V.I. Telnov, arXiv:physics/0604108
5. D.L. Borden, D.A. Bauer, D.O. Caldwell, Phys. Rev. D **48**, 4018 (1993)
6. K. Moenig, A. Rosca, arXiv:hep-ph/0506271
7. F. Bechtel et al., arXiv:physics/0601204
8. P. Niezurawski, arXiv:hep-ph/0503295
9. P. Niezurawski, arXiv:hep-ph/0507004
10. P. Niezurawski, A.F. Zarnecki, M. Krawczyk, arXiv:hep-ph/0507006
11. R.M. Godbole, arXiv:hep-ph/0604228
12. M.G. Albrow, A. Rostovtsev, arXiv:hep-ph/0009336
13. V.A. Khoze, A.D. Martin, M.G. Ryskin, Eur. Phys. J. C **23**, 311 (2002)
14. A. De Roeck, V.A. Khoze, A.D. Martin, R. Orava, M.G. Ryskin, Eur. Phys. J. C **25**, 391 (2002)
15. B.E. Cox, AIP Conf. Proc. **753**, 103 (2005) [arXiv:hep-ph/0409144]
16. J. Ellis, J.S. Lee, A. Pilaftsis, Phys. Rev. D **71**, 075 007 (2005)
17. M.G. Albrow et al., CERN-LHCC-2005-025
18. A.D. Martin, V.A. Khoze, M.G. Ryskin, arXiv:hep-ph/0507305
19. A.D. Martin, V.A. Khoze, M.G. Ryskin, W.J. Stirling, Gribov Memorial Volume, Quarks, Hadrons and Strong Interactions, Y.L. Dokshitzer, P. Levai, J. Nyiri (Eds.), (World Scientific, 2006), pp. 129–144 [arXiv:hep-ph/0507040]
20. M. Boonekamp, R. Peschanski, C. Royon, Phys. Lett. B **598**, 243 (2004) and references therein
21. A.V. Kisselev, V.A. Petrov, R.A. Ryutin, arXiv:hep-ph/0506034 and references therein
22. A.B. Kaidalov, V.A. Khoze, A.D. Martin, M.G. Ryskin, Eur. Phys. J. C **33**, 261 (2004)
23. V.A. Khoze, A.D. Martin, M.G. Ryskin, Eur. Phys. J. C **14**, 525 (2000)
24. For a recent review see, J.R. Forshaw, arXiv:hep-ph/0508274
25. V.A. Khoze, A.D. Martin, M.G. Ryskin, Eur. Phys. J. C **18**, 167 (2000)
26. E. Gotsman, E. Levin, U. Maor, E. Naftali, A. Prygarin, arXiv:hep-ph/0511060
27. V.A. Khoze, A.D. Martin, M.G. Ryskin, arXiv:hep-ph/0006005, In: Proc. of 8th Int. Workshop on Deep Inelastic Scattering and QCD (DIS2000), Liverpool, ed. by J. Gracey, T. Greenshaw (World Scientific, 2001), p. 592
28. V.A. Khoze, A.D. Martin, M.G. Ryskin, Eur. Phys. J. C **19**, 477 (2001)
29. V.A. Khoze, A.D. Martin, M.G. Ryskin, Eur. Phys. J. C **20**, 599 (2001) (erratum)
30. J. Kalliopuska et al. In: HERA and the LHC: a workshop on the implications of HERA for LHC physics, Proc., S. Alekhin et al. CERN-2005-014, DESY-PROC-2005-01, December 2005, p. 448, arXiv:hep-ph/0601013
31. S. Heinemeyer, V.A. Khoze, M.G. Ryskin, W.J. Stirling, M. Tasevsky, G. Weiglein, in preparation
32. V.A. Khoze, A.D. Martin, M.G. Ryskin, Eur. Phys. J. C **34**, 327 (2004)
33. M. Arneodo et al., In: HERA and the LHC: a workshop on the implications of HERA for LHC physics, Proc., S. Alekhin et al., CERN-2005-014, DESY-PROC-2005-01, December 2005, p. 455, arXiv:hep-ph/0601013
34. B.E. Cox et al., Eur. Phys. J. C **45**, 401 (2006)
35. V.A. Khoze, M.G. Ryskin, W.J. Stirling, Eur. Phys. J. C **44**, 227 (2005)
36. J.F. Gunion, H.E. Haber, Phys. Rev. D **48**, 5109 (1993)
37. K.A. Isparin, I.A. Nagorskaya, A.G. Oganesian, V.A. Khoze, Yad. Fiz. **11**, 1278 (1970) [Sov. J. Nucl. Phys. **11**, 712 (1970)]
38. V.A. Khoze, arXiv:hep-ph/9504348
39. D.L. Borden, V.A. Khoze, W.J. Stirling, J. Ohnemus, Phys. Rev. D **50**, 4499 (1994)
40. V.S. Fadin, V.A. Khoze, A.D. Martin, Phys. Rev. D **56**, 484 (1997)
41. S.J. Parke, T.R. Taylor, Phys. Rev. Lett. **56**, 2459 (1986)
42. F.A. Berends, W.T. Giele, Nucl. Phys. B **306**, 759 (1988)
43. M.L. Mangano, S.J. Parke, Phys. Rep. **200**, 301 (1991)
44. S. Soldner-Rembold, G. Jikia, Nucl. Instrum. Methods A **472**, 133 (2001) [arXiv:hep-ex/0101056]
45. J. Monk, A. Pilkington, arXiv:hep-ph/0502077
46. M. Boonekamp, C. Hogg, J. Monk, A. Pilkington, M. Tasevsky, In: HERA and the LHC: a Workshop on the implications of HERA for LHC physics, Proc., S. Alekhin et al., CERN-2005-014, DESY-PROC-2005-01, December 2005, p. 487, arXiv:hep-ph/0601013
47. CDF Collaboration, K. Goulianos, arXiv:hep-ex/0507072
48. CDF Collaboration – Run II, M. Gallinaro, arXiv:hep-ph/0505159
49. V.A. Khoze, A.D. Martin, M.G. Ryskin, Eur. Phys. J. C **26**, 229 (2002)
50. W.A. Bardeen, A.J. Buras, D.W. Duke, T. Muta, Phys. Rev. D **18**, 3998 (1978)
51. E. Braaten, J.P. Leveille, Phys. Rev. D **22**, 715 (1980)
52. M. Drees, K.I. Hikasa, Phys. Lett. B **240**, 455 (1990)
53. M. Drees, K.I. Hikasa, Phys. Rev. D **41**, 1547 (1990)

54. R. Kleiss, Z. Kunszt, W.J. Stirling, Phys. Lett. B **253**, 269 (1991)
55. A.L. Kataev, V.T. Kim, Mod. Phys. Lett. A **9**, 1309 (1994)
56. G. Jikia, A. Tkabladze, Phys. Rev. D **54**, 2030 (1996)
57. M. Melles, W.J. Stirling, Phys. Rev. D **59**, 094009 (1999)
58. M. Melles, W.J. Stirling, Eur. Phys. J. C **9**, 101 (1999)
59. M. Melles, W.J. Stirling, Nucl. Phys. B **564**, 325 (2000)
60. M. Melles, W.J. Stirling, V.A. Khoze, Phys. Rev. D **61**, 054015 (2000)
61. V.V. Sudakov, Sov. Phys. JETP **3**, 65 (1956) [Zh. Eksp. Teor. Fiz. **30**, 87 (1956)]
62. Z. Bern, L.J. Dixon, D.C. Dunbar, D.A. Kosower, Nucl. Phys. B **435**, 59 (1995)
63. A. Brandhuber, S. McNamara, B.J. Spence, G. Travaglini, JHEP **0510**, 011 (2005)
64. Z. Kunszt, A. Signer, Z. Trocsanyi, Nucl. Phys. B **411**, 397 (1994)
65. C. Anastasiou, E.W.N. Glover, C. Oleari, M.E. Tejeda-Yeomans, Nucl. Phys. B **605**, 486 (2001)
66. C. Anastasiou, E.W.N. Glover, M.E. Tejeda-Yeomans, Nucl. Phys. B **629**, 255 (2002)
67. L. Dixon, private communication
68. A.D. Martin, R.G. Roberts, W.J. Stirling, R.S. Thorne, Eur. Phys. J. C **14**, 133 (2000)
69. F.A. Berends, R. Kleiss, P. De Causmaecker, R. Gastmans, T.T. Wu, Phys. Lett. B **103**, 124 (1981)
70. F.E. Low, Phys. Rev. **110**, 974 (1958)
71. T.H. Burnett, N.M. Kroll, Phys. Rev. Lett. **20**, 86 (1968)
72. Y.L. Dokshitzer, V.A. Khoze, W.J. Stirling, Nucl. Phys. B **428**, 3 (1994)
73. V.A. Khoze, A.D. Martin, M.G. Ryskin, arXiv:hep-ph/0605113
74. Y.L. Dokshitzer, F. Fabbri, V.A. Khoze, W. Ochs, Eur. Phys. J. C **45**, 387 (2006)